Systematic analysis of occurrence of equatorial noise emissions using 10 years of data from the Cluster mission

Z. Hrbackova, O. Santolík, F. Nemec, E. Macusova, Nicole Cornilleau-Wehrlin

AGU PUBLICATIONS

JGR

Journal of Geophysical Research: Space Physics

RESEARCH ARTICLE

10.1002/2014JA020268

Key Points:
- Systematic analysis shows magnetosonic equatorial noise at L from 2.5 to 8.5
- Occurrence peaks at 15 MLT in the plasmatrough, no peak in the plasmasphere
- Around equator, occurrence rates reach 40%, and they reach over 60% for high Kp

Correspondence to:
O. Santolík,
os@ufa.cas.cz

Citation:
Hrbáčková, Z., O. Santolík, F. Němec, E. Macúšová, and N. Cornilleau-Wehrlin (2015), Systematic analysis of occurrence of equatorial noise emissions using 10 years of data from the Cluster mission, *J. Geophys. Res. Space Physics*, *120*, 1007–1021, doi:10.1002/2014JA020268.

Received 6 JUN 2014
Accepted 30 DEC 2014
Accepted article online 8 JAN 2015
Published online 7 FEB 2015

Systematic analysis of occurrence of equatorial noise emissions using 10 years of data from the Cluster mission

Z. Hrbáčková[1,2], O. Santolík[1,2], F. Němec[2], E. Macúšová[1], and N. Cornilleau-Wehrlin[3,4]

[1]Department of Space Physics, Institute of Atmospheric Physics CAS, Prague, Czech Republic, [2]Faculty of Mathematics and Physics, Charles University in Prague, Prague, Czech Republic, [3]LPP/CNRS, Palaiseau, France, [4]LESIA/Observatoire de Paris, Meudon, France

Abstract We report results of a systematic analysis of equatorial noise (EN) emissions which are also known as fast magnetosonic waves. EN occurs in the vicinity of the geomagnetic equator at frequencies between the local proton cyclotron frequency and the lower hybrid frequency. Our analysis is based on the data collected by the Spatio-Temporal Analysis of Field Fluctuations–Spectrum Analyzer instruments on board the four Cluster spacecraft. The data set covers the period from January 2001 to December 2010. We have developed selection criteria for the visual identification of these emissions, and we have compiled a list of more than 2000 events identified during the analyzed time period. The evolution of the Cluster orbit enables us to investigate a large range of McIlwain's parameter from about $L \sim 1.1$ to $L \sim 10$. We demonstrate that EN can occur at almost all analyzed L shells. However, the occurrence rate is very low (<6%) at L shells below $L = 2.5$ and above $L = 8.5$. EN mostly occurs between $L = 3$ and $L = 5.5$, and within 7° of the geomagnetic equator, reaching 40% occurrence rate. This rate further increases to more than 60% under geomagnetically disturbed conditions. Analysis of occurrence rates as a function of magnetic local time (MLT) shows strong variations outside of the plasmasphere (with a peak around 15 MLT), while the occurrence rate inside the plasmasphere is almost independent on MLT. This is consistent with the hypothesis that EN is generated in the afternoon sector of the plasmapause region and propagates both inward and outward.

1. Introduction

Equatorial noise (EN), also referred to as fast magnetosonic waves, are intense magnetospheric emissions coupled to the whistler mode branch. These emissions propagate in the extraordinary mode nearly perpendicular to the static magnetic field in a frequency range from the ion cyclotron frequency to the lower hybrid frequency. The magnetic field fluctuations of this wave mode are linearly polarized along the static magnetic field direction. The electric field fluctuations, on the other hand, are elliptically polarized in the plane perpendicular to the static magnetic field. *Russel et al.* [1970] first predicted the importance of these waves for the acceleration mechanism of electrons in the outer radiation belt.

More detailed observations of EN emissions were reported by *Gurnett* [1976]. He detected a fine structure of EN which was not previously seen in the data with a lower resolution. The waves that appeared to be noisy and unstructured in the low-resolution frequency-time spectrograms were found to consist of many spectral lines with frequency spacings from a few hertz to several tens of hertz. These lines were suggested to result from an ion-cyclotron harmonic interaction [*Gurnett*, 1976]. Energetic protons at energies ~10 keV with the ring-like distribution function at pitch angles close to 90° were observed in association with these waves [*Curtis and Wu*, 1979; *Perraut et al.*, 1982; *Boardsen et al.*, 1992]. They are believed to provide the energy required for the wave generation during the magnetic storms [*Horne et al.*, 2000]. *Chen et al.* [2010, 2011] obtained similar results using a simulation of magnetosonic wave instability and observational analysis of the proton ring distribution. They found that proton ring distribution can provide a source of free energy for exciting EN waves when the ring velocity is within a factor of 2 above or below the Alfvénic speed.

Horne et al. [2007] found that the EN emissions can efficiently resonate with higher pitch angles electrons. They are therefore unlikely causing losses in the outer radiation belt by pitch angle diffusion into the loss cone and precipitation. However, they can cause electron acceleration from a few keV to MeV energies. It seems that acceleration and pitch angle scattering of electrons are much less efficient during the solar minimum conditions than during the solar maximum [*Shprits et al.*, 2013], possibly also due to the very

low intensity of EN. On the other hand, *Meredith et al.* [2009] found that the losses of relativistic electrons in the inner slot region are most likely due to the combined effects of hiss and guided whistlers. However, under active conditions, magnetosonic waves may be as important in this process as guided whistlers. Additionally, *Mourenas et al.* [2013] found that the fast magnetosonic waves can influence electron lifetimes and acceleration both inside and outside the plasmasphere, mainly at the lower end of their frequency range.

Laakso et al. [1990] and *Kasahara et al.* [1994] demonstrated that EN emissions can occur at radial distances from about 2 to 7 R_E and at geomagnetic latitudes up to about 10° from the geomagnetic equator. EN has the most intense magnetic field fluctuations among all natural emissions in the relevant interval of frequencies and latitudes, with occurrence rates reaching 60% [*Santolík et al.*, 2004]. Most intensity peaks of a Gaussian model of the power spectral density (PSD) of EN occur within 2° of the dipole magnetic equator [*Němec et al.*, 2005]. The emissions appear to be the most intense in the noon to afternoon sector [*Green et al.*, 2005]. However, outside the plasmapause on L shells up to 4.5, intense emissions were reported at most magnetic local times, and their average intensity further increases with magnetic activity [*Meredith et al.*, 2008]. *Tsurutani et al.* [2014] found that the occurrence rates of magnetosonic waves increase with the geomagnetic activity and that these waves inside the plasmasphere occur at all local times with a slight preference for the midnight-postmidnight sector. *Ma et al.* [2013] observed these waves with occurrence rates of 20%, mainly outside of the plasmapause on the dawnside. They also noticed shifting of the occurrence pattern toward earlier local time during geomagnetically active periods.

A ray tracing study by *Kasahara et al.* [1994] showed that EN emissions can propagate azimuthally around the plasmapause. Radial propagation in the equatorial plane was examined in latter studies by *Horne et al.* [2000] and *Santolík et al.* [2002]. These emissions can also propagate inward and outward, crossing the plasmapause boundary [*Xiao et al.*, 2012]. *Chen and Thorne* [2012] investigated exactly perpendicular propagation in an azimuthally symmetrical magnetosphere. They confirmed azimuthal as well as radial propagation. Moreover, they identified two classes of EN emissions—trapped and untrapped. Trapped waves propagate over a broad range of the magnetic local time (MLT) due to the presence of the plasmapause. A recent study by *Němec et al.* [2013] has shown that azimuthal angles of the wave propagation are strongly influenced by the local plasma density. They found that all directions of propagation are detected inside the plasmasphere while the wave propagation outside the plasmapause (in the plasmatrough) is predominantly westward or eastward.

We report results of a systematic study of EN emissions observed by the Cluster spacecraft. Using a very large database of 10 years of measurements, we mainly address questions for which contradictory answers can be found in the literature: What are the occurrence rates of EN emissions in the plasmasphere and in the plasmatrough? How the occurrence rates in these two regions depend on MLT and geomagnetic activity?

Unlike most similar studies, we have visually inspected all the relevant data and identified time intervals when EN emissions were observed. This enables us to study the occurrence of these emissions with unmatched details. A brief description of the data set, examples of EN observations, and selection criteria used for the identification of EN are given in section 2. Spatial distribution of the occurrence of EN and its relation to the geomagnetic activity is presented in section 3. Occurrence of EN in the plasmasphere and plasmatrough regions is described in section 4.The results are discussed in section 5 and summarized in section 6.

2. Data Set and Selection Criteria

We have used the data measured by the Electric Fields and Waves (EFW) experiment and by the Spatio-Temporal Analysis of Field Fluctuations experiment (STAFF) on board the Cluster spacecraft from January 2001 to December 2010. The EFW experiment utilizes four spherical probes placed on 50 m long wire booms [*Gustafsson et al.*, 1997] for two-axis measurements of the electric field in the spacecraft spin plane. The STAFF experiment consists of a three-axis search coil magnetometer at the end of a 5 m long boom, a waveform unit, and a Spectrum Analyzer (STAFF-SA).

STAFF-SA combines the three magnetic components from the magnetometer and the two electric components from the EFW instrument to obtain 5×5 Hermitian spectral matrices. These are calculated at

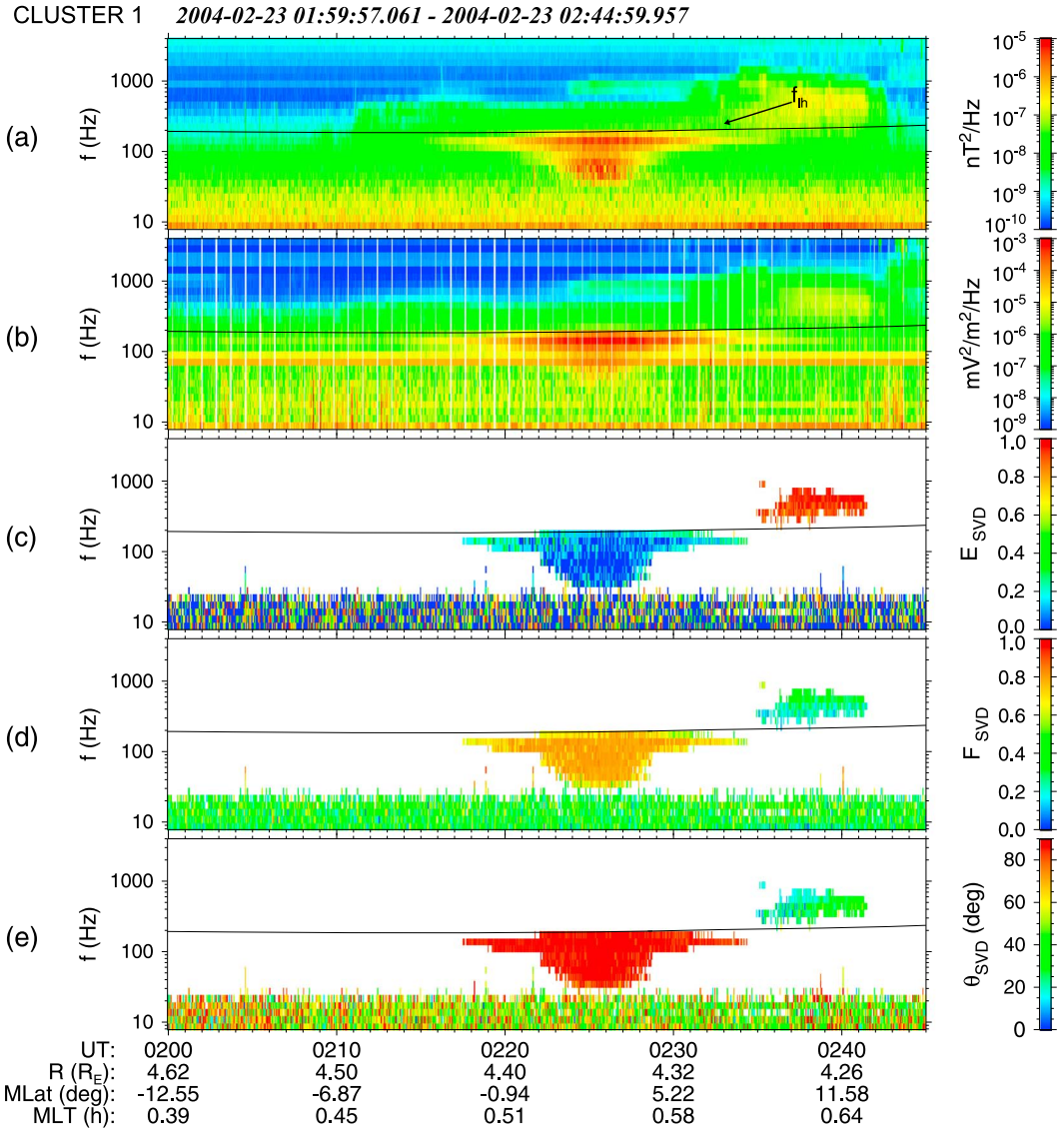

Figure 1. An example of the EN emission observed by Cluster 1 on 23 February 2004 between 02:00 and 02:45 UT. (a) Sum of the PSD of the three magnetic components, (b) sum of the PSD of the two electric components, (c) ellipticity E of the magnetic field fluctuations, (d) planarity F of the magnetic field fluctuations, and (e) polar angle theta θ of the wave vector direction relative to the ambient magnetic field. Universal time (UT) and position of the spacecraft are given on the bottom of the figure: radial distance in Earth radii (R_E), geomagnetic dipole latitude in degrees, and MLT in hours. Maximum possible value of the local lower hybrid frequency (f_{lh}) is overplotted in Figures 1a–1e. The data in Figures 1c–1e are shown only for the frequency-time intervals with the PSD of the magnetic field fluctuations larger than 10^{-7} nT^2 Hz^{-1} and the PSD of the electric field fluctuations larger than 10^{-6} mV^2 m^{-2} Hz^{-1}.

27 frequencies distributed logarithmically in the frequency range between 8 Hz and 4 kHz [*Cornilleau-Wehrlin et al.*, 1997, 2003]. In the most frequent normal measurement mode, the time resolution is 1 s for power spectral densities (main diagonal elements of the spectral matrices) and 4 s for phases and coherence (off-diagonal elements of the spectral matrices).

Figure 1 shows an example of a typical EN event. It was observed by Cluster 1 on 23 February 2004 around 02:25 UT when the spacecraft was crossing the equatorial plane close to its perigee on the nightside. The data were recorded in the low-latitude region within 10° from the geomagnetic equator at a radial distance of about 4.4 R_E. The black solid curves in the panels represent the lower hybrid frequency (f_{lh}) which is the maximum frequency limit for the EN emissions. Its value is estimated as the geometric average of the proton and electron cyclotron frequencies assuming a dense hydrogen plasma.

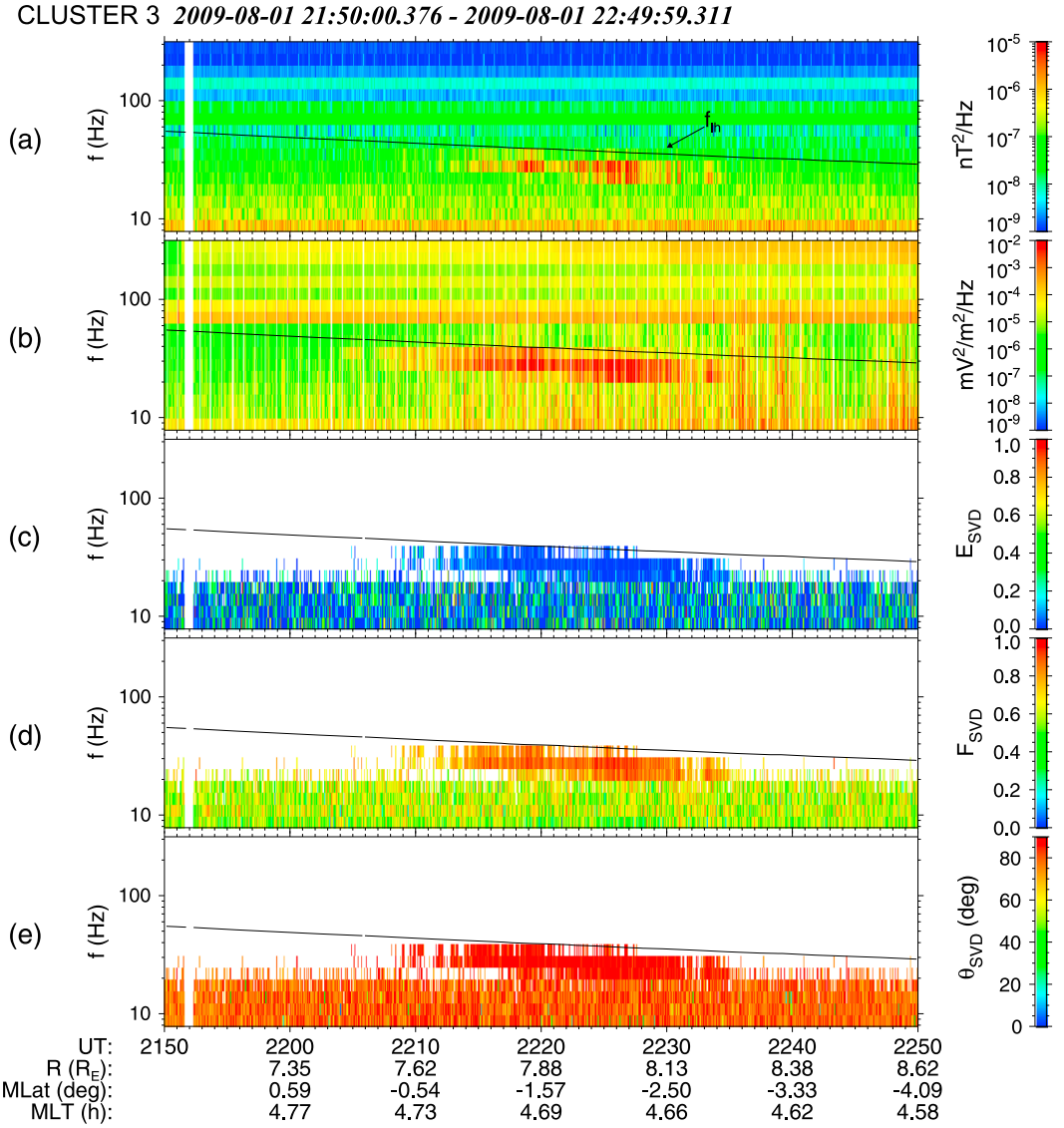

Figure 2. An example of the EN emission observed by Cluster 3 on 1 August 2009 between 21:50 and 22:50 UT. The meaning of the individual panels is the same as in Figure 1.

The maximum PSD of the magnetic field fluctuations corresponding to this event is around 2×10^{-6} nT^2 Hz^{-1} (Figure 1a), and the maximum PSD of the electric field fluctuations is around 7×10^{-4} mV^2 m^{-2} Hz^{-1} (Figure 1b). The emission occurs approximately between 30 Hz and 220 Hz, with the maximum frequency limit at the anticipated value of the lower hybrid frequency.

Figure 1c shows the absolute value of the ellipticity of the magnetic field fluctuations corresponding to this event. The ellipticity is calculated from the singular value decomposition (SVD) of the magnetic spectral matrix as the ratio of the two largest axes of the polarization ellipsoid [*Santolík et al.*, 2003, equation (13)]. The zero ellipticity represents the linear polarization. The magnetic field of this emission is linearly polarized, which is consistent with the wave propagation in the extraordinary mode [*Stix*, 1992].

Planarity F (Figure 1d) is calculated from the SVD method of the magnetic spectral matrix [*Santolík et al.*, 2003, equation (12)]. The values close to 1 represent waves polarized nearly in a single plane.

The polar angle θ shown in Figure 1e denotes a direction of the wave vector with respect to the ambient magnetic field. The value close to 90° corresponds to the direction perpendicular to the ambient magnetic field.

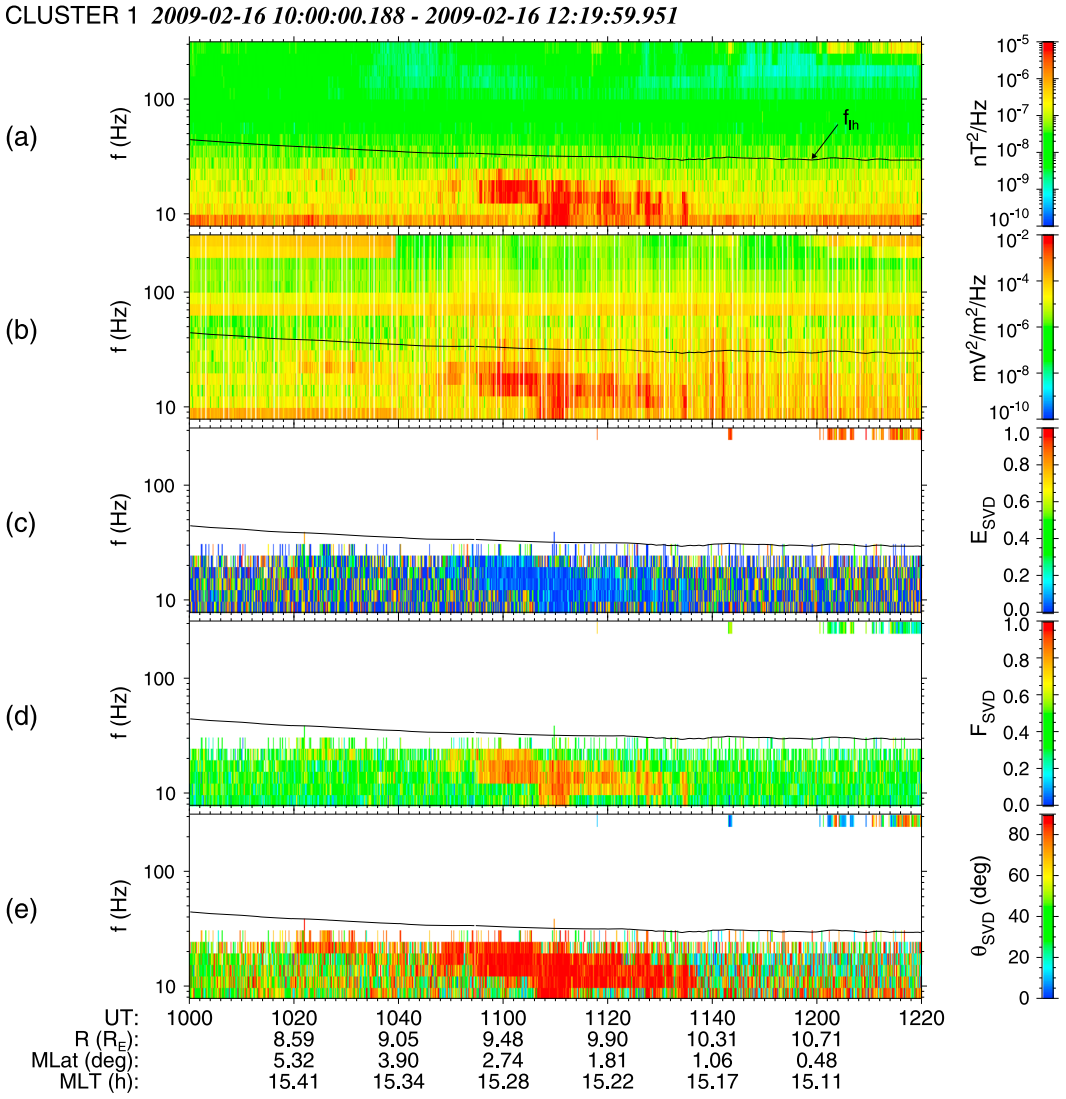

Figure 3. An example of the EN emission observed by Cluster 1 on 16 February 2009 between 10:00 and 12:20 UT. The meaning of the individual panels is the same as in Figure 1.

Note that results in Figures 1c–1e are calculated only for the frequency-time intervals with the PSD of the magnetic field fluctuations larger than 10^{-7} nT^2 Hz^{-1} and the PSD of the electric field fluctuations larger than 10^{-6} mV^2 m^{-2} Hz^{-1}.

In order to perform a systematic analysis of the occurrence of EN, we have prepared a list of time intervals when the emissions were observed (a database of EN events). We have started with a list of all Cluster equatorial crossings. The STAFF-SA data corresponding to each of the crossings have been visually checked for the presence of the events that fulfill predefined selection criteria based on the systematic analysis of EN emissions during the first 2 years of the Cluster mission [*Santolík et al.*, 2004; *Němec et al.*, 2005]:

1. EN is an electromagnetic emission. We have used a threshold 10^{-7} nT^2 Hz^{-1} for the PSD of the magnetic field fluctuations and a threshold 10^{-6} mV^2 m^{-2} Hz^{-1} for the PSD of the electric field fluctuations. The intensity of any emission to be considered as EN has to exceed both these thresholds.
2. The PSDs of the electric and magnetic field fluctuations have their respective local maxima within 7° from the dipole geomagnetic equator.
3. Magnetic field fluctuations corresponding to EN are nearly linearly polarized. The absolute value of the ellipticity of magnetic field fluctuations determined by the SVD method of *Santolík et al.* [2003] must be lower than 0.2.

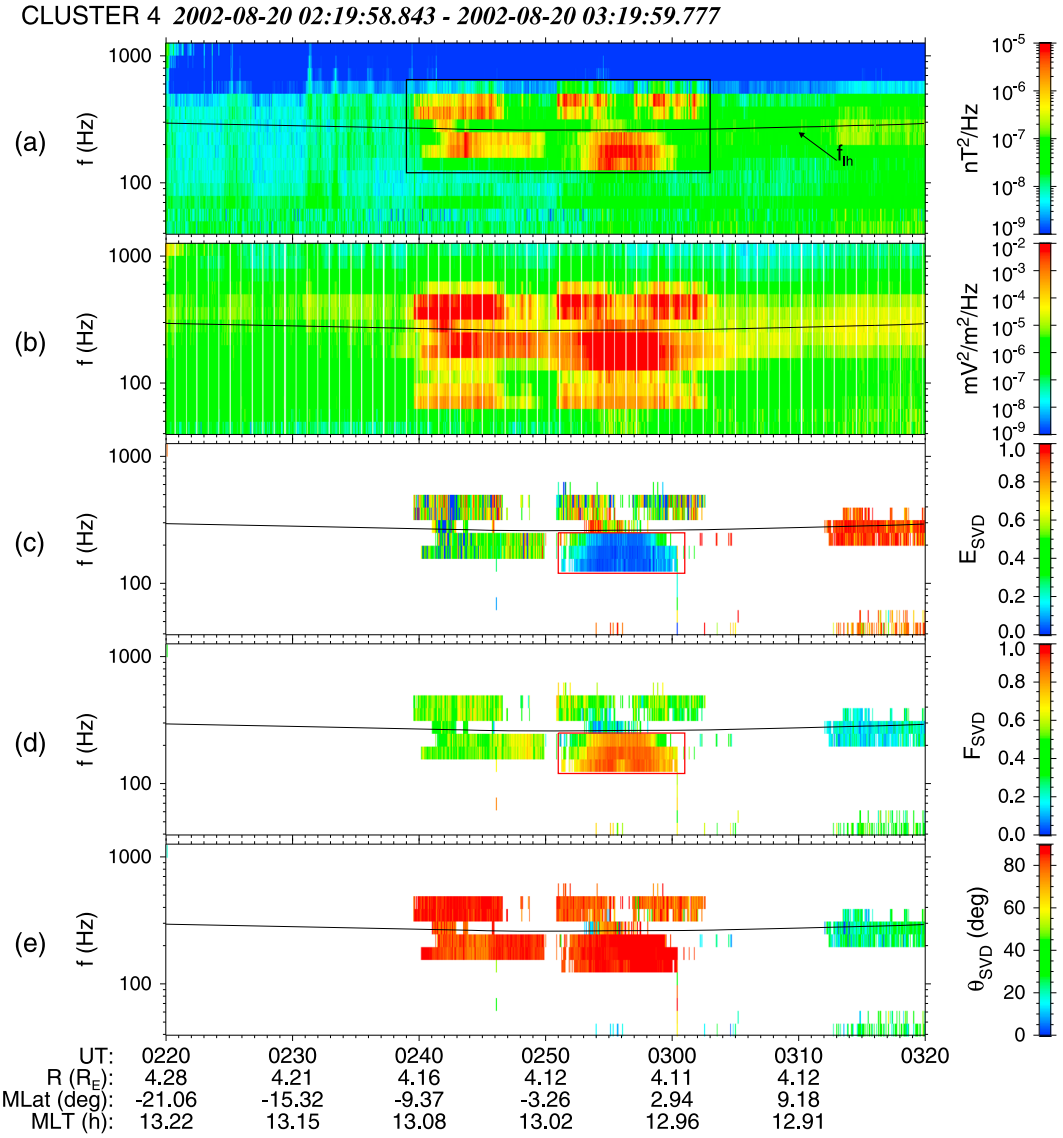

Figure 4. An example of the EN emission observed by Cluster 4 on 20 August 2002 between 02:20 and 03:20 UT. The meaning of the individual panels is the same as in Figure 1.

We use the data set containing the orbital information which has 1 min time resolution. For each of the identified EN events and for each of the Cluster spacecraft, we have recorded the initial time and the final time.

Examples of emissions measured by Cluster 3 on 1 August 2009 and by Cluster 1 on 16 February 2009 at exceptionally large radial distances from 7.5 R_E to 10.5 R_E are shown in Figures 2 and 3 for the local morning and afternoon, respectively. The satellites were well outside of the plasmasphere during these two measurement intervals. The maxima of PSD of the magnetic field fluctuations corresponding to these two events, respectively, were around 9×10^{-7} nT^2 Hz^{-1} (Figure 2a) and 2×10^{-6} nT^2 Hz^{-1} (Figure 3a). The maxima of PSD of the electric field fluctuations corresponding to these two events, respectively, were around 10^{-3} mV^2 m^{-2} Hz^{-1} (Figure 2b) and 10^{-2} mV^2 m^{-2} Hz^{-1} (Figure 3b). The maximum frequency is very low for both these events (around 30 Hz). High-density approximation used for the estimation of the lower hybrid frequency is not valid at these large radial distances. However, it is still useful as an upper estimate of f_{lh} and therefore as the upper frequency limit of EN.

The last example shows an emission which does not seem to have the typical EN form (Figure 4). It was recorded by Cluster 4 on 20 August 2002 in the dayside MLT sector. The maximum PSD of the magnetic

Table 1. Summary of the EN Emissions Detected Between January 2001 and December 2010

	Equator Crossings	Events	Occurrence Rate (%)	L Shells
2001	396	202	51	3.8–4.5
2002	521	242	46	4.0–5.0
2003	586	344	59	3.9–4.9
2004	580	305	53	4.0–4.8
2005	576	375	65	3.9–5.3
2006	575	289	50	3.5–4.9
2007	563	230	41	2.6–4.0
2008	547	105	19	2.1–3.4, 8.9–10.0
2009	655	25	4	1.4–2.5, 6.1–10.0
2010	786	89	11	1.1–2.0, 3.2–10.0
Total	5785	2229	40	1.1–10.0
Total 01–06	3234	1772	54	3.5–5.3

field fluctuations corresponding to the event is around 2×10^{-6} nT^2 Hz^{-1} (Figure 4a), and the maximum PSD of the electric field fluctuations is around 2×10^{-2} mV^2 m^{-2} Hz^{-1} (Figure 4b). The emission occurs approximately between 100 Hz and 300 Hz.

According to the first two selection criteria, it seems that EN emission occurs over the whole time interval from 2:39 UT to 3:02 UT marked by a black rectangle in Figure 4a. However, there are two facts which are worth noticing. First, f_{lh} goes through the emission and divides it into two bands. Second, the ellipticity is larger than 0.2 for the waves outside the red rectangle in Figure 4c, and the planarity is close to 1 only in the red rectangle in Figure 4d. Based on the third selection criterion, we have therefore included only the waves inside the red rectangle to our database of EN events. The waves outside this rectangle also have very high wave vector angles between 70 and 90° (Figure 4e). They might be hypothetically generated by a similar mechanism as the EN emissions, but their planarity is only between 0.3 and 0.7 (Figure 4d), indicative of a mixture of waves with different wave vectors. By strictly using the ellipticity criterion, we exclude similar unclear cases from our analysis. Note that the planarity and the wave vector angle do not belong to the selection criteria, but they can be used to verify if the observed wave properties correspond to the wave properties expected for EN emissions.

3. Occurrence of EN

We have analyzed 5785 satellite crossings of the geomagnetic equator at L shells from $L = 1.1$ to $L = 10$ from January 2001 to December 2010. The statistics for all the analyzed years is summarized in Table 1. Note that there are four Cluster spacecraft and each of them was taken as an independent data source, i.e., the overall results were calculated by using all of them.

The column "equator crossings" includes the crossings of the geomagnetic equator for which the measurements of magnetic field fluctuations were available from the STAFF instrument. Intervals in the column "L shells" have been calculated for data from the column equator crossings, and they show ranges of L shells where the Cluster spacecraft measured EN emissions at the geomagnetic equator during the corresponding year.

Altogether, 2229 EN events have been identified. Table 1 shows that the percentage of orbits with EN events remains approximately constant from the beginning of the mission until 2006 (46–65%). Since 2006 it starts to decrease systematically down to less than 20% during the years 2008–2010. This can be explained by taking into account the evolution of the spacecraft orbit. Until 2006 the orbits remained approximately identical (see column L shells), with equatorial crossings close to the perigee at a radial distance of about 4 R_E. Since 2007, the orbit changed significantly. Starting 2008, we present two ranges of L shells which show equatorial crossings close to the perigee (the first range) and also crossings close to the apogee (the second range). The new perigee radial distance has been typically in the range of about 1.1 to 3 R_E. The inclination of the orbit has become lower, and the distant equator crossings have moved inward to a typical distance of about 7 to 12 R_E. This allowed us to occasionally detect EN emissions twice during a single orbit. As we demonstrate later, the occurrence rate of EN is very low at L shells less than 2.5 and larger than 8.5,

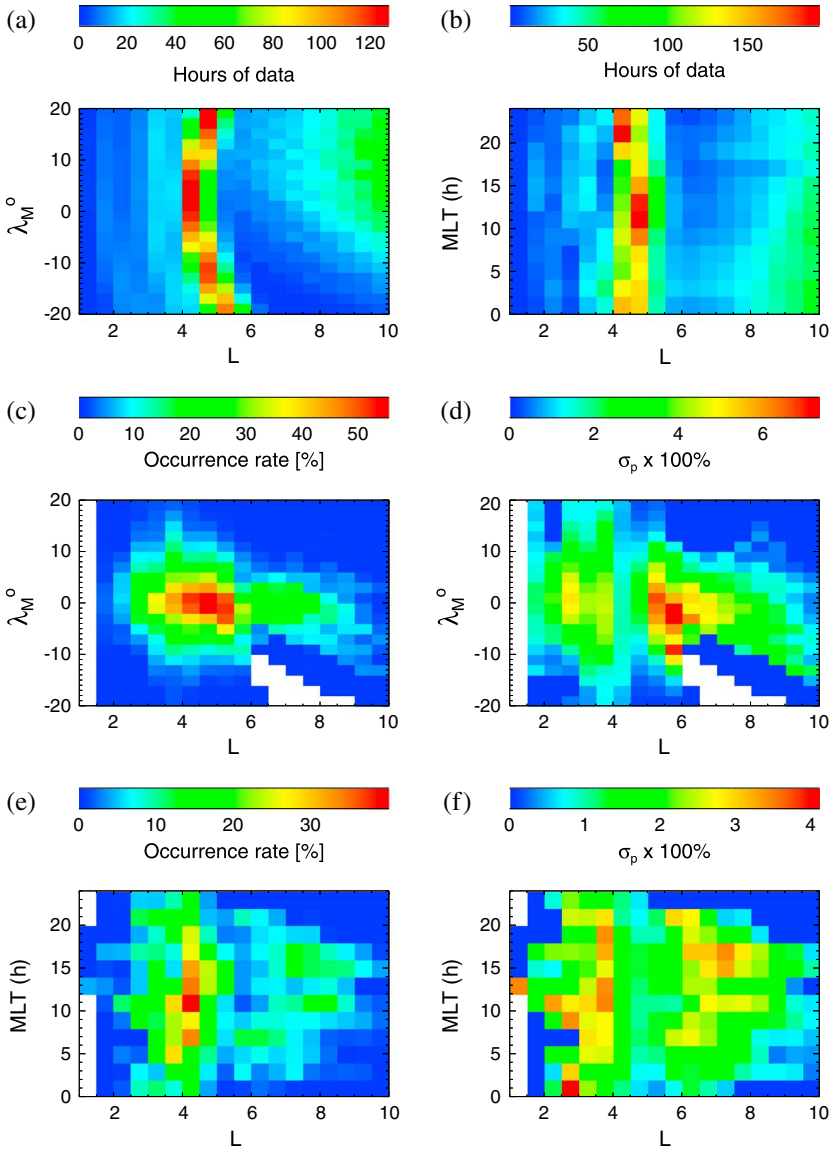

Figure 5. Coverage of Cluster STAFF-SA measurements given in number of hours spent in bins of (a) 0.5 $L \times 2°$ λ_M and (b) 0.5 $L \times 2$ h MLT. Occurrence rates of EN and their estimated standard deviations σ_P in the same bins of (c, d) $L \times \lambda_M$ and (e, f) $L \times$ MLT. White areas correspond to a coverage inferior to 3 h of data in a given bin.

which explains the lower occurrence of EN during the later years of the mission. The average percentage of orbits with EN emissions is 54% during the years 2001–2006.

With this data set, we analyze the occurrence of EN emissions as a function of L shell and geomagnetic latitude (λ_M). Figure 5a shows the coverage of the L-λ_M plane (for all MLT) by the STAFF-SA measurements during the entire analyzed interval; λ_M values are limited to the interval between −20° and 20°, and the coverage of the McIlwain's parameter is analyzed between $L = 1.1$ and $L = 10$. Figure 5b shows the orbital coverage in the L-MLT plane (for λ_M from −20° to 20°). The entire MLT range has been covered, but the orbit has been mostly limited within $L = 4$–6 in this interval of λ_M. This is connected to the time interval before 2006. Later development of the orbit gave much wider coverage, but some regions are still purely covered. Figure 5c presents occurrence rates (ORs) of EN as a function of L and λ_M. OR is obtained from the number of minutes spent in a given bin while observing EN emissions using the normalization by the orbital coverage from Figure 5a. The results show that OR can reach up to 60% in the L shell range between 4 and 5.5.

Note that OR is only calculated when the coverage is larger than 180 min of data, corresponding to 180 measurement points. The same lower limit of data coverage is also used in the following OR calculations. The standard deviations σ_P of the obtained occurrence rates P can be estimated from the properties of the binomial distribution,

$$\sigma_P \approx \sqrt{\frac{P(1-P)}{N d}}, \tag{1}$$

where $N \geq 180$ is the number of measurement points and d is an average fraction of independent points in our data set. The 1 min data points from a single orbit are measured under similar conditions, but their level of independence is very difficult to determine. A rough estimate of a typical time scale of EN variations, as they are scanned by the Cluster orbit, gives us a value of ≈4 min (see Figures 1–4).

Another aspect of this problem is linked to the fact that we independently use the data of all four Cluster spacecraft in our analysis. The spatial separations of the spacecraft differed during different operational phases of the Cluster mission. These variations resulted in time differences of equatorial passages of the different spacecraft which range from tens of seconds up to hundreds of minutes. Similarly, differences in positions in the equatorial plane range from a few kilometers up to thousands of kilometers. As noted by *Němec et al.* [2005], some of the data points from the different spacecraft can be considered as independent, but the independence of data from short separation periods is questionable. A rough estimate gives us an average number of two independent data points from four spacecraft during the analyzed period.

With these estimates, we effectively obtain $4 \times 2 = 8$ times less independent data points compared to their original number, and hence, $d \approx 1/8$. Note that this rough estimate of d is good enough for obtaining representative results since σ_P depends on $\sqrt{d}$. The resulting values of σ_P for OR from Figure 5c are shown in Figure 5d. We can see that the maximum values are only several units per cent, demonstrating thus a high statistical significance of the obtained occurrence rates.

A combined OR as a function of MLT and L shell is shown in Figure 5e, while the standard deviations estimated according to equation (1) are given in Figure 5f. The occurrence for $L \geq 5$ appears significantly higher during the local day than during the local night, while the distribution in MLT seems to be more uniform in the interval of L shells below $L = 5$. Histograms of OR as a function of L shell are shown in Figures 6a and 6b. Figure 6a shows the data analyzed within the entire interval of magnetic latitudes as it was used in Figure 5, i.e., within 20° from the geomagnetic equator. Figure 6b corresponds to the interval of the geomagnetic latitude within 7° from the geomagnetic equator. Three quarters of the time intervals in which the EN emissions were observed are entirely contained in this narrower interval. There is therefore a generally lower occurrence rate in Figure 6a than in Figure 6b because it includes a wider interval of geomagnetic latitudes and hence more records without EN events. The same thresholds for data coverage as in Figure 5 (3 h of data) have been used, and the results have been plotted for all data (black line), for geomagnetically calm times (red line), and geomagnetically disturbed times (blue line). Error bars show standard deviations estimated according to equation (1). EN mostly occurs between $L = 3$ and $L = 5.5$, reaching 40% occurrence rate within 7° of the geomagnetic equator (Figure 6b). For L just below 5.5, OR reaches more than 70% during geomagnetically disturbed times. Maximum occurrence rates obtained during the disturbed times are found at L just below 4 for a wider latitudinal interval (Figure 6a). There is only a very small overall occurrence rate of EN below $L = 1.5$. The occurrence rates also gradually decrease at L shells between 5.5 and 10. During disturbed times, this decrease is more pronounced, with very small OR at L above 7. The distributions for calm periods are similar to the distributions for the entire data set.

4. Analysis of EN Emissions Inside and Outside the Plasmasphere

With the same data set, we will further analyze the EN emissions occurrence inside and outside the plasmasphere as a function of geomagnetic latitude (λ_M) and MLT. We use three models to determine the location of the plasmapause. The first one is the CA1992 model of *Carpenter and Anderson* [1992] which is dependent on the maximum value of the *Kp* index in previous 24 h. *O'Brien and Moldwin* [2003] implement a different method to account for the dependence on the Earth's magnetic activity, and they additionally also use a dependence on MLT (OM2003 model). We also use the PPCH2012 model by *Heilig and Lühr* [2013, equation (6)], which includes a quadratic dependence on *Kp* and a more complex dependence on MLT than the other two models.

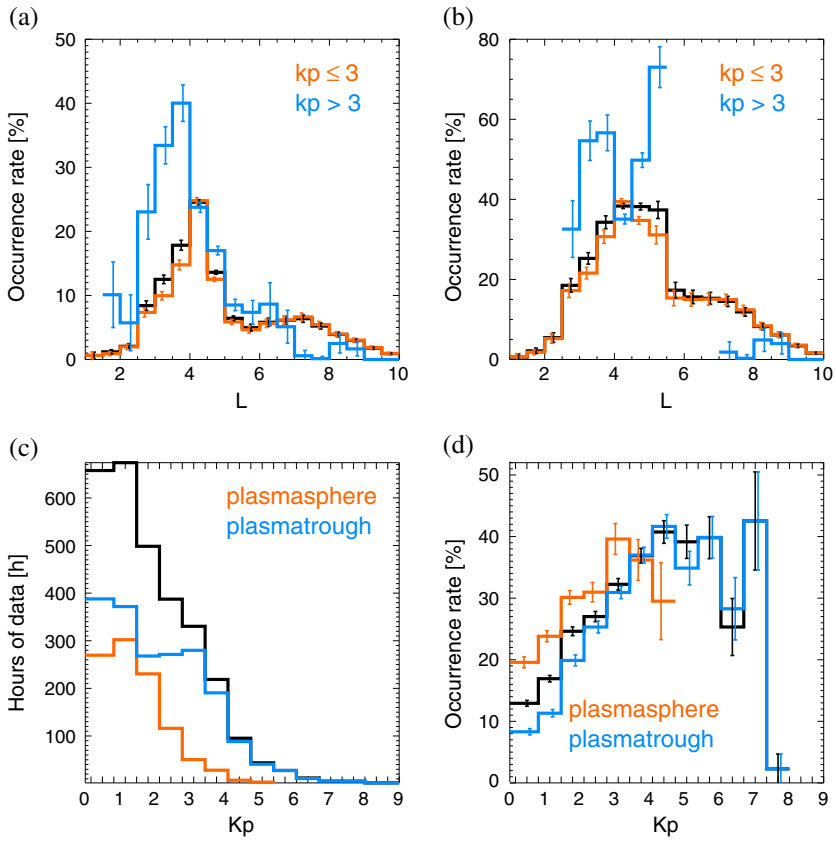

Figure 6. (a) Occurrence rate of EN as a function of L shell for $|\lambda_M| < 20°$ (black line: the entire data set, red line: subset of data for low geomagnetic activity $Kp \leq 3$, and blue line: subset of data for high geomagnetic activity $Kp > 3$). (b) Occurrence rate of EN as a function of L shell for $|\lambda_M| < 7°$ (the same color coding as in Figure 6a). (c) Distribution of *Kp* index for all equatorial passages, $|\lambda_M| < 7°$ (black line: the entire data set, red line: subset of plasmaspheric data inside the PPCH2012 plasmapause model, and blue line: subset of data in the plasmatrough outside the PPCH2012 plasmapause model). (d) OR of EN as the function of *Kp* for data within $|\lambda_M| < 7°$ (the same color coding as in Figure 6c). Error bars show the estimated standard deviations σ_P.

For a typical example of EN (Figure 1), we can compare the results of the plasmapause location between these three models and the real measurements from the WHISPER (Waves of High Frequency and Sounder for Probing of Electron Density by Relaxation experiment) instruments onboard Cluster [*Décréau et al.*, 1997]. The data from WHISPER were not available for Cluster 1, but all spacecraft followed approximately the same orbit, so we use the available measurements from Cluster 2. When we define the plasmapause boundary by the electron density exceeding 80 particles/cm^3 (corresponding to a plasma frequency ~80 kHz at the upper frequency limit of the WHISPER instruments), these measurements show that the satellite entered the plasmasphere at 2:10 at $L = 4.6$ and left it at 2:44 at $L = 4.5$. The plasmapause locations calculated from the models were at $L = 4.2$ (CA1992 model), $L = 4.8$ (OM2003 model), and $L = 4.4$ (PPCH2012 model). OM2003 and PPCH2012 models are therefore closest to the real plasmapause position and the observed EN emission from Figure 1 (at $L = 4.4$) is located close to the plasmapause boundary according to all models.

Figure 6c shows a distribution of *Kp* index for passages within 7° from the geomagnetic equator in the whole interval of L shells (1.1–10) for data measured both inside and outside of the model plasmapause. The results are similar for the three plasmapause models (CA1992, OM2003, and PPCH2012), and we therefore only show results based on the PPCH2012 model. Resulting OR of the EN emissions as the function of *Kp* is shown in Figure 6d. The highest occurrence of EN is observed during disturbed magnetic conditions (for *Kp* from 3+ to 7). For these conditions, however, the shape of the Cluster orbit implies that we have only a very limited orbital coverage inside the plasmasphere.

Figure 7 shows the orbital coverage and OR as a function of λ_M and MLT. We include here all the analyzed values of the McIlwain's parameter between $L = 1.1$ and $L = 10$, but we separately give the results obtained

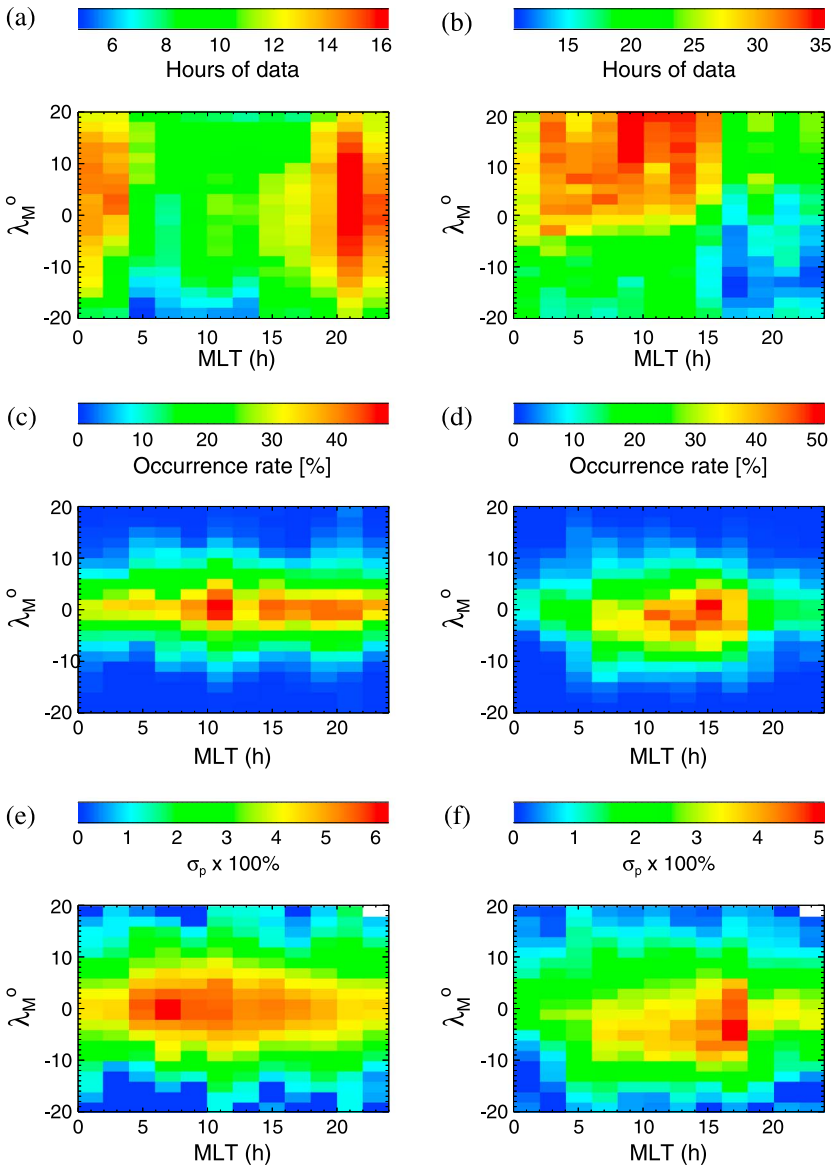

Figure 7. Coverage of Cluster STAFF-SA measurements: number of hours spent in bins of 2 h MLT × 2° λ_M (a) inside the plasmasphere according to PPCH2012 model and (b) outside of the plasmasphere. Occurrence rates of EN and their estimated standard deviations σ_P, respectively, (c, e) inside the plasmasphere and (d, f) outside of the plasmasphere.

in the plasmasphere (Figures 7a, 7c, and 7e) and in the plasmatrough (Figures 7b, 7d, and 7f). The obtained results are again similar for the three above mentioned plasmapause models. We therefore only show results based on the PPCH2012 model. We can note that we have a good coverage in this case and that OR of EN is significantly dependent on MLT outside of the plasmasphere, with a peak occurrence of 50% at the equator in the early afternoon sector and with the lowest equatorial OR of 10% just after the local midnight. This MLT variation reaches more than 4 standard deviations around the average value. Inside the plasmasphere we can note fluctuations of a peak OR approximately between 30% and 45–50%. A shallow minimum in the early morning sector can be noticed, but a clear, globally pronounced dependence on MLT is absent, with variations reaching less than 2 standard deviations around the average value.

The dependence of the data coverage and OR on MLT is shown in detail in Figure 8 for λ_M within 7° from the geomagnetic equator. The presented results are again shown for data in the plasmasphere (Figures 8a and 8c) and in the plasmatrough (Figures 8b and 8d) but, in this case, also for two different levels of

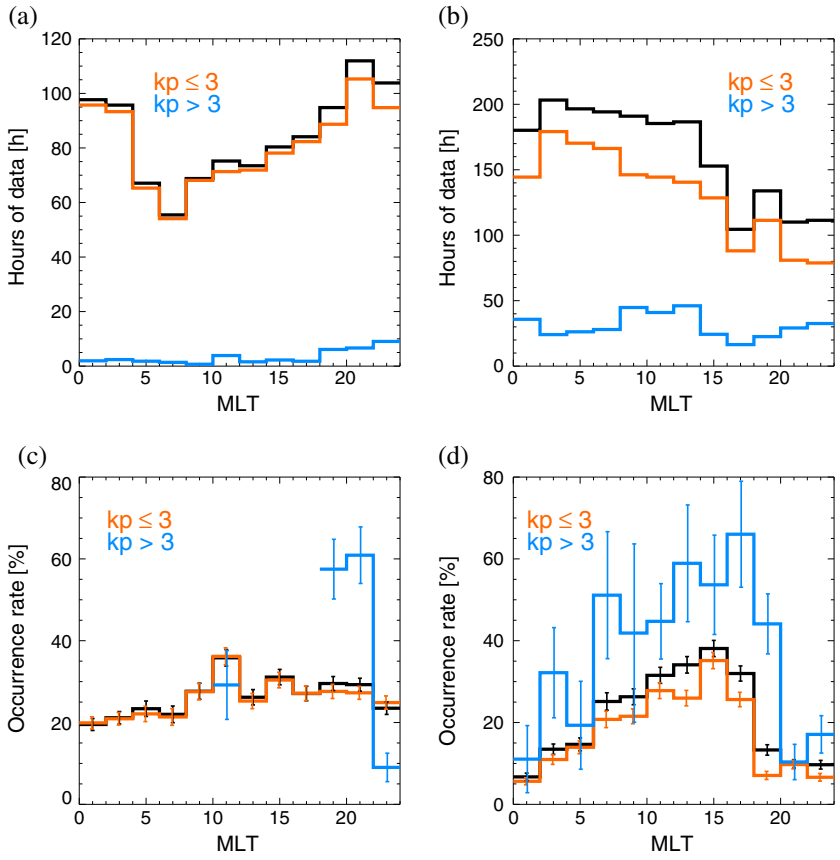

Figure 8. (a) Coverage of Cluster STAFF-SA measurements given in numbers of hours spent in bins of 2 h MLT inside the plasmasphere according to the PPCH2012 model; (b) the same as in Figure 8a but for the data in the plasmatrough outside of the plasmasphere; and occurrence rate of the EN emissions as a function of MLT for data (c) inside the plasmasphere and (d) outside of the plasmasphere. Error bars show the estimated standard deviations σ_P.

geomagnetic activity. The plasmaspheric results do not show a pronounced variation of OR as a function of MLT, reaching values between 20% and 35%, with a shallow minimum of the nightside and maximum on the dayside. A very limited coverage for data inside the plasmasphere can be again noted during geomagnetically disturbed times.

On the other hand, a strong dependence on MLT is obvious outside the plasmasphere. A higher overall OR (more than 30%) is obtained between 10 and 18 h, and the maximum OR (nearly 40%) is found around 15 h of MLT. OR around the midnight (below ~15%) is less then one half of its maximum value. This variation is again very significant with respect to the estimated error bars. OR is generally higher during the geomagnetically disturbed times compared to the quiet times, reaching over 65% in the afternoon sector, but a very similar MLT dependence is observed.

5. Discussion

We have used 10 years of observations of EN emissions by the four Cluster spacecraft to compile a large database of EN events. We use exact quantitative criteria (locations of the maximum PSDs, intensity, and ellipticity thresholds) for the identification of events, combined with a careful visual inspection of the spectrograms.

The presented set of the three selection criteria was compiled in agreement with previous results of *Santolík et al.* [2004, Figures 2 and 5–7]. We also used the dipole model for the determination of the geomagnetic latitude. However, the true geomagnetic equator should be defined by the magnetic field minimum along a particular field line [*Němec et al.*, 2006]. Since the dipole model becomes inaccurate at larger radial distances where significant deviations from the dipole are present, we extended the range of the second

criterion from 5° (used by *Santolík et al.* [2004]) up to 7° of the absolute geomagnetic latitude in order not to eliminate EN emissions above $L = 7$.

However, *Tsurutani et al.* [2014] observed magnetosonic waves as far from the equator as 20° or 60° but with lower intensities. The selection criterion of having a local maximum of PSD within 7° of the geomagnetic latitude intentionally removes these magnetosonic waves which are occasionally observed at higher latitudes from our data set, concentrating thus our analysis only at the frequent phenomenon which corresponds to earlier observations of equatorial noise. By integration of the occurrence rates of EN as a function of latitude in Figures 5 or 7, we find that more than 90% of our data points are limited within 10° from the geomagnetic dipole equator, and more than 60% of our data points occur within 5° from the geomagnetic equator.

The main advantage of our data set, however, is a combination of polarization and intensity criteria. Only the data corresponding to EN with low ellipticity of the magnetic field polarization are selected and included in this study. This was not possible in the previous studies [*Green et al.*, 2005; *Meredith et al.*, 2008; *Pokhotelov et al.*, 2008] which consider only the PSD in a given interval of frequencies and latitudes.

The percentage of orbits with EN emissions that we have observed during the years 2001–2006 when Cluster was crossing the equator at radial distances of about 4 R_E can be compared to the result of *Santolík et al.* [2004]. They visually inspected 781 1–3 h data intervals around the perigee passages. The data within 10° were available for 671 cases, and the resulting occurrence rate of EN was about 60%. OR is lower in the present paper, it is only 49% during the first 2 years. The reason is that every passage for which data are available at the geomagnetic equator is counted as "equator passage" in Table 1, without requiring the data coverage up to 10°. We therefore analyze a higher number of equatorial Cluster passages in the present study.

We have analyzed data inside and outside the plasmasphere separately. We use three models to obtain the location of the plasmapause—CA1992, OM2003, and PPCH2012. The results for these models are similar. We also separate the results for different levels of geomagnetic activity. We are unable to draw any conclusions from cases inside the plasmasphere for $Kp > 3+$ where we have only a very limited orbital coverage (unlike for Time History of Events and Macroscale Interactions during Substorms observations by *Ma et al.* [2013]). On the other hand, we have a good orbital coverage in the plasmatrough outside of the plasmasphere where we observe almost twice higher OR in the plasmatrough outside of the plasmasphere for these disturbed times, compared to plasmatrough cases with $Kp \leq 3+$.

As it is discussed above, the OR of the EN emissions is only very weakly dependent on MLT inside the plasmasphere (Figure 8c), taking into account our experimental uncertainties. However, outside of the plasmasphere (Figure 8d), OR is significantly larger on the dayside. These results are roughly consistent with the surveys by *Pokhotelov et al.* [2008] and *Ma et al.* [2013], but they are not consistent with the overall results on EN intensities by *Green et al.* [2005] and especially with the results obtained by *Meredith et al.* [2008]. All these studies identified EN emissions only on a basis of a predefined frequency interval, without taking into account the wave polarization properties. They therefore might include also other emissions than EN (most probably plasmaspheric hiss and/or whistlers) into their statistical results. *Green et al.* [2005] analyzed the data from the Dynamics Explorer and IMAGE missions in the frequency range from 30 to 300 Hz up to $L \sim 4$ inside the plasmasphere. Their results show a similar dependence of intensities on MLT as we found it for OR from Cluster data outside the plasmasphere. *Meredith et al.* [2008] analyzed the wave electric intensity in the frequency range $0.5f_{lh} < f < f_{lh}$ using data from the CRRES satellite. They found these waves at most MLTs for data outside of the plasmasphere, but the waves were mainly found in the afternoon sector in the data set localized inside the plasmasphere. *Pokhotelov et al.* [2008] processed data from the Cluster mission in the frequency range $0.0005 \leq f/f_{ce} < 0.02$ from $L \sim 4$ to $L \sim 9$. This mostly corresponds to locations outside the plasmasphere. They found a similar dependence on MLT as in our study. On the other hand, we were unable to reproduce the shift of peak occurrences toward dawn indicated by *Ma et al.* [2013] for higher geomagnetic activity: we do not observe any such effect outside of the plasmasphere, and the limited Cluster orbital coverage for disturbed conditions prevents us from reliably verifying it inside the plasmasphere.

Němec et al. [2013] suggest from their analysis that EN emissions are generated close to the plasmapause density gradient. This hypothesis is consistent with our results taking into account results of the ray

tracing analysis by *Chen and Thorne* [2012]. They obtain much lower spread of the MLT values for observations outside the plasmasphere [*Chen and Thorne*, 2012, Figure 4] than inside the plasmasphere where the EN emissions are trapped. This explains our observations of OR of the EN emissions, assuming that source region is in the afternoon sector.

6. Conclusion

We have presented a systematic study of the EN emissions observed by the Cluster spacecraft between the local proton cyclotron frequency and the local lower hybrid frequency. This study is based on the data measured by the STAFF-SA instrument during 10 years of operation (from January 2001 to December 2010). We have used three selection criteria for the identification of EN: (i) intensity thresholds for both electric and magnetic field fluctuations, (ii) location of the maxima of the PSDs relative to the geomagnetic equator, and (iii) linear polarization of the magnetic field fluctuations.

Using these criteria, we have identified EN events that occurred during the analyzed time period. Altogether, we have analyzed 5785 equator crossings. Among these, we have identified 2229 cases of EN emissions. The change of the Cluster orbit during the analyzed period allowed us to study the occurrence of EN over a large range of L shells from about 1.1 to 10. EN emissions were found to occur at all analyzed L shells. However, the EN emissions are mostly observed at L shells from about 3 to 5.5. On the other hand, the OR at L shells less than $L = 2.5$ and larger than $L = 8.5$ is very low (< 6%). EN is mostly (in more than 90% of cases) confined within 10° from the geomagnetic dipole equator. EN emissions occur more often during disturbed geomagnetic conditions between $Kp = 3+$ and $Kp = 7$.

We have studied the dependence of OR of EN on MLT separately for data inside and outside the plasmasphere. We demonstrate that the occurrence depends on MLT outside the plasmasphere. Maximum OR (30–40% or more than 65% during geomagnetically disturbed times) is observed during the daytime (from 10 to 18 h MLT), with a peak around 15 h, while the lowest OR is found around the midnight (from 22 to 2 h MLT). Inside the plasmasphere, we find that OR is only very weakly dependent of the MLT.

These results are consistent with a speculative hypothesis that the source of EN is localized close to the plasmapause [*Němec et al.*, 2013] on the dayside, with a peak occurrence in the early afternoon sector. According to the ray tracing results of *Chen and Thorne* [2012], EN waves can propagate in a narrower MLT interval at high L shells. They can therefore stay more often localized on the dayside. At lower L shells, EN waves can effectively propagate in the azimuthal direction and their resulting occurrence is therefore much more equalized with respect to MLT. Further analysis of the source locations is needed to verify this hypothesis.

Acknowledgments
The authors acknowledge additional support from grants GAUK 678212, Kontakt II LH12231, and GACR P209/12/P658 and EU support through the FP7-Space grant agreement 284520 for the MAARBLE collaborative research project. The data used to produce the results of this paper can be obtained from the ESA Cluster Science Archive (http://cosmos.esa.int/csa).

Michael Balikhin thanks the reviewers for their assistance in evaluating this paper.

References

Boardsen, S. A., D. L. Gallagher, D. A. Gurnett, W. K. Peterson, and J. L. Green (1992), Funnel-shaped, low-frequency equatorial waves, *J. Geophys. Res.*, *97*(A10), 14,967–14,976.

Carpenter, D. L., and R. R. Anderson (1992), An ISEE/whistler model of equatorial electron density in the magnetosphere, *J. Geophys. Res.*, *97*(A2), 1097–1108.

Chen, L., and R. M. Thorne (2012), Perpendicular propagation of magnetosonic waves, *Geophys. Res. Lett.*, *39*, L14102, doi:10.1029/2012GL052485.

Chen, L., R. M. Thorne, V. K. Jordanova, and R. B. Horne (2010), Global simulation of magnetosonic waves instability in the storm time magnetosphere, *J. Geophys. Res.*, *115*, A11222, doi:10.1029/2010JA015707.

Chen, L., R. M. Thorne, V. K. Jordanova, M. F. Thomsen, and R. B. Horne (2011), Magnetosonic wave instability analysis for proton ring distributions observed by the LANL magnetospheric plasma analyzer, *J. Geophys. Res.*, *116*, A03223, doi:10.1029/2010JA016068.

Cornilleau-Wehrlin, N., et al. (1997), The Cluster Spatio-Temporal Analysis of Field Fluctuations (STAFF) experiment, *Space Sci. Rev.*, *79*, 107–136.

Cornilleau-Wehrlin, N., et al. (2003), First results obtained by the Cluster STAFF experiment, *Ann. Geophys.*, *21*, 437–456.

Curtis, S. A., and C. S. Wu (1979), Gyroharmonic emissions induced by energetic ions in the equatorial plasmasphere, *J. Geophys. Res.*, *84*, 2597–2607.

Décréau, P. M. E., et al. (1997), Whisper, a resonance sounder and wave analyser: Performances and perspectives for the Cluster mission, *Space Sci. Rev.*, *79*, 157–193.

Green, J. L., S. Boardsen, L. Garcia, W. W. L. Taylor, S. F. Fung, and B. W. Reinisch (2005), On the origin of whistler mode radiation in the plasmasphere, *J. Geophys. Res.*, *110*, A03201, doi:10.1029/2004JA010495.

Gurnett, D. A. (1976), Plasma wave interactions with energetic ions near the magnetic equator, *J. Geophys. Res.*, *81*, 2765–2770.

Gustafsson, G., et al. (1997), The electric field and wave experiment for the Cluster mission, *Space Sci. Rev.*, *79*, 137–156.

Heilig, B., and H. Lühr (2013), New plasmapause model derived from CHAMP field-aligned current signatures, *Ann. Geophys.*, *31*, 529–539.

Horne, R. B., G. V. Wheeler, and H. S. C. K. Alleyne (2000), Proton and electron heating by radially propagating fast magnetosonic waves, *J. Geophys. Res.*, *105*(A12), 27,597–27,610.

Horne, R. B., R. M. Thorne, S. A. Glauert, N. P. Meredith, D. Pokhotelov, and O. Santolík (2007), Electron acceleration in the Van Allen radiation belts by fast magnetosonic waves, *Geophys. Res. Lett.*, *34*, L17107, doi:10.1029/2007GL030267.

Kasahara, Y., H. Kenmochi, and I. Kimura (1994), Propagation characteristics of the ELF emissions observed by the satellite Akebono in the magnetic equatorial region, *Radio Sci.*, *29*, 751–767.

Laakso, H., H. Junginger, A. Roux, R. Schmidt, and C. de Villedary (1990), Magnetosonic waves above f_{cH+} at geostationary orbit: GEOS 2 results, *J. Geophys. Res.*, *95*, 10,609–10,621.

Ma, Q., W. Li, R. M. Thorne, and V. Angelopoulos (2013), Global distribution of equatorial magnetosonic waves observed by THEMIS, *Geophys. Res. Lett.*, *40*, 1895–1901, doi:10.1002/grl.50434.

Meredith, N. P., R. B. Horne, S. A. Glauert, D. N. Baker, S. G. Kanekal, and J. M. Albert (2009), Relativistic electron loss timescales in the slot region, *J. Geophys. Res.*, *114*, A03222, doi:10.1029/2008JA013889.

Meredith, N. P., R. B. Horne, and R. R. Anderson (2008), Survey of magnetosonic waves and proton ring distributions in the Earth's inner magnetosphere, *J. Geophys. Res.*, *113*, A06213, doi:10.1029/2007JA012975.

Mourenas, D., A. V. Artemyev, O. V. Agapitov, and V. Krasnoselskikh (2013), Analytical estimates of electron quasilinear diffusion by fast magnetosonic waves, *J. Geophys. Res. Space Physics*, *118*, 3096–3112, doi:10.1002/jgra.50349.

Němec, F., O. Santolík, K. Gereová, E. Macúšová, Y. de Conchy, and N. Cornilleau-Wehrlin (2005), Initial results of a survey of equatorial noise emissions observed by the Cluster spacecraft, *Planet. Space Sci.*, *53*, 291–298.

Němec, F., O. Santolík, K. Gereová, E. Macúšová, H. Laakso, Y. de Conchy, M. Maksimovic, and N. Cornilleau-Wehrlin (2006), Equatorial noise: Statistical study of its localization and the derived number density, *Adv. Space Res.*, *37*, 610–616.

Němec, F., O. Santolík, J. S. Pickett, Z. Hrbáčková, and N. Cornilleau-Wehrlin (2013), Azimuthal directions of equatorial noise propagation determined using 10 years of data from the Cluster spacecraft, *J. Geophys. Res. Space Physics*, *118*, 7160–7169, doi:10.1002/2013JA019373.

O'Brien, T. P., and M. B. Moldwin (2003), Empirical plasmapause models from magnetic indices, *Geophys. Res. Lett.*, *30*(4), 1152, doi:10.1029/2002GL016007.

Perraut, S., A. Roux, P. Robert, R. Gendrin, J.-A. Sauvaud, J.-M. Bosqued, G. Kremser, and A. Korth (1982), Systematic study of ULF waves above Fu+ from GEOS 1 and 2 measurements and their relationships with proton ring distributions, *J. Geophys. Res.*, *87*, 6219–6236.

Pokhotelov, D., F. Lefeuvre, R. B. Horne, and N. Cornilleau-Wehrlin (2008), Survey of ELF-VLF plasma waves in outer radiation belt observed by Cluster STAFF-SA experiment, *Ann. Geophys.*, *26*, 3269–3277.

Russel, C. T., R. E. Holzer, and E. J. Smith (1970), OGO 3 Observations of ELF noise in the magnetosphere, *J. Geophys. Res.*, *75*, 755–768.

Santolík, O., J. S. Pickett, D. A. Gurnett, M. Maksimovic, and N. Cornilleau-Wehrlin (2002), Spatiotemporal variability and propagation of equatorial noise observed by Cluster, *J. Geophys. Res.*, *107*(A12), 1495, doi:10.1029/2001JA009159.

Santolík, O., M. Parrot, and F. Lefeuvre (2003), Singular value decomposition methods for wave propagation analysis, *Radio. Sci.*, *38*(1), 1010, doi:10.1029/2000RS002523.

Santolík, O., F. Němec, K. Gereová, E. Macúšová, Y. de Conchy, and N. Cornilleau-Wehrlin (2004), Systematic analysis of equatorial noise below the lower hybrid frequency, *Ann. Geophys.*, *22*, 2587–2595.

Shprits, Y. Y., A. Runov, and B. Ni (2013), Gyro-resonant scattering of radiation belt electrons during the solar minimum by fast magnetosonic waves, *J. Geophys. Res. Space Physics*, *118*, 648–652, doi:10.1002/jgra.50108.

Stix, T. H. (1992), *Waves in Plasmas*, Am. Inst. of Phys., New York.

Tsurutani, B. T., B. J. Falkowski, J. S. Pickett, O. P. Verkhoglyadova, O. Santolik, and G. S. Lakhina (2014), Extremely intense ELF magnetosonic waves: A survey of polar observations, *J. Geophys. Res. Space Physics*, *119*, 964–977, doi:10.1002/2013JA019284.

Xiao, F., Q. Zhou, Z. He, and L. Tang (2012), Three-dimensional ray tracing of fast magnetosonic waves, *J. Geophys. Res.*, *117*, A06208, doi:10.1029/2012JA017589.